Effect of Reaction Parameters on Composition and Morphology of Titanate Nanomaterials

ARTICLE *in* THE JOURNAL OF PHYSICAL CHEMISTRY C · JULY 2009

Impact Factor: 4.77 · DOI: 10.1021/jp903195h

5 AUTHORS, INCLUDING:

Nadine Millot
University of Burgundy
62 PUBLICATIONS **763** CITATIONS
SEE PROFILE

Lucien Saviot
University of Burgundy
111 PUBLICATIONS **1,804** CITATIONS
SEE PROFILE

R. Chassagnon
University of Burgundy
27 PUBLICATIONS **237** CITATIONS
SEE PROFILE

Effect of Reaction Parameters on Composition and Morphology of Titanate Nanomaterials

Anne-Laure Papa, Nadine Millot,* Lucien Saviot, Rémi Chassagnon, and Olivier Heintz

Institut Carnot de Bourgogne, UMR 5209 CNRS - Université de Bourgogne, BP 47870, 21078 Dijon cedex, France

Received: April 7, 2009; Revised Manuscript Received: May 14, 2009

In the present article, we report the synthesis of titanate nanotubes and nanoribbons with controlled morphology, structure, and chemical composition depending on the main parameters of the synthesis. Hydrothermal processing time, grain size of the precursor, type of agitation, and acid treatment were investigated, and the principal controversies mentioned in the literature such as nanotube crystallographic structure, their chemical composition, and acid treatment impact are discussed. These controversies may be due to the heterogeneities present in all the samples and are rarely considered in the literature. These nanostructures were characterized by Raman spectroscopy, X-ray photoelectron spectroscopy, X-ray diffraction (XRD), and transmission electron microscopy. A careful desummation of the first XRD peaks revealed the presence of both nanosheets and nanotubes and allowed an estimation of their proportions. In addition, the titanate nanotube section is observed to be not perfectly circular but rather elliptic. Moreover, the first acid treatment effect is shown to remove any trace of sodium and structural water. The second effect of acid washing is a morphological evolution.

1. Introduction

A new route for the synthesis of TiO_2-derived nanotubes was presented by Kasuga et al.[1,2] The precursors used were nanopowders of either anatase or rutile, treated in hydrothermal and strongly basic conditions (NaOH aqueous solution at 110 °C over 20 h). The resulting product was tubelike in shape, open-ended, and had a multilayer morphology rolled up in spiral. The diameter of this tubular material was around 10 nm, with lengths reaching a few hundred nanometers. Since this pioneering study, the mechanistic aspect of the synthesis of titanate nanotubes (TNT) has not been studied extensively, despite several promising applications such as reversible storage of hydrogen,[3] anodes for rechargeable lithium batteries,[4−6] photocatalysis,[7] photovoltaic cells,[8,9] sensors,[10] and bioapplications.[11,12]

TNT can be formed with a temperature ranging from 100 to 180 °C when the starting precursors are powders of TiO_2 (anatase and/or rutile).[13] From transmission electron microscopy (TEM) observations, the yield of nanotubes synthesized increases between 100 and 150 °C and decreases for higher temperature.[14] It also increases with the synthesis duration. For example, at 150 °C, Thorne et al. reported that the yield, estimated by TEM, changes from 0 to 80% when synthesis time varies from 2 to 72 h.[14] The concentration of sodium hydroxide is also an important factor for the tube formation. Indeed, sticks (short tubes) are obtained when it is lower than 5 mol/L or higher than 20 mol/L.[13] In addition, a maximum amount of nanotubes was obtained when the concentration ranged from 10 to 15 mol/L. Their adsorption surfaces can reach up to 350 m^2/g.

In their pioneering work, Kasuga et al. reported that the crystalline raw material is initially converted to an amorphous product during the alkaline treatment; the nanotubes would be formed after hydrochloric acid treatment and washings with distilled water. These authors consequently concluded that the acid treatment, which follows the hydrothermal synthesis, is a critical stage for the nanotube formation process. They concluded by selected area electron diffraction (SAED) and Raman spectroscopy that the crystalline phase of their nanotubes was anatase. Du et al. used the same hydrothermal process in NaOH (10 mol/L) at 130 °C and obtained nanotubes with an average diameter of 8−10 nm and lengths reaching a few hundred nanometers without HCl washings.[15,16] Their results thus contradicted the assumption of Kasuga et al. regarding the essential acid-washing step. In addition, according to their analyses by X-ray diffraction (XRD) and SAED, they concluded that the resulting phase was not TiO_2 anatase but $H_2Ti_3O_7$ (monoclinic system) and that the tubes had a multiwall morphology with interlayer spacing of 0.75−0.78 nm. In 2007, Li et al. found that, after shortly washing with nitric acid and water, some halfway curled nanofoils were formed and after thorough washing a large quantity of tubular materials was obtained.[17]

Chen et al. tried to obtain nanotubes by using other bases (KOH, LiOH) and also NaCl.[16] Their tests did not succeed. According to them, it would be thus essential to have simultaneously strong concentrations of sodium cations and hydroxide ions, which would act as catalysts. Then, Kukovecz et al. obtained trititanate nanotubes using a 10 mol/L Na_2S solution as the reactional medium.[18] Chen et al. also showed that nanotubes were obtained regardless of the size and the structure of the precursor if the starting material is crystalline.[16] Afterward, Ma et al. synthesized nanotubes by considerably reducing the time of synthesis to 4 h thanks to one-hour sonication before hydrothermal treatment.[19]

Concerning the phase and the composition, after acid treatment and washings with distilled water, the phase obtained by XRD is often $H_2Ti_4O_9 \cdot H_2O$.[20] Other more exotic phases were reported, such as $H_xTi_{2-x/4}\square_{x/4}O_4$ ($x \approx 0.7$, $\square$ = vacancy), known as lepidocrocite phase by Ma et al. in 2003,[21] $H_2Ti_5O_{11} \cdot H_2O$ (nanoribbons) by Yuan and Su in 2004,[13] $Na_xH_{2-x}Ti_3O_7$, $x \approx 0.75$ by Sun and Li in 2003,[22] and finally, $H_{1.5}Na_{0.5}Ti_3O_7$ by Yoshida et al. in 2005.[23] Strong disparities and contradictions

* To whom correspondence should be addressed. Telephone: +33380395937. Fax: +33380396167. E-mail: nadine.millot@u-bourgogne.fr.

10.1021/jp903195h CCC: $40.75
Published on Web 06/19/2009

TABLE 1: Phase-Specific Surface Area and Grain Size of the Different Precursors[a]

precursors	SC1 (tt 12 h, 470 °C)	SC2 (tt 2 h, 500 °C)	P25 (Degussa)		rutile (Tioxide)	
phase	anatase	anatase	anatase + rutile		rutile	
S_{BET} (m^2/g) (±5%)	94.0	86.0	50.0		6.6	
$Ø_{BET}$ (nm) (±5%)	16.4	18.0	21.0		214.0	
$Ø_{DRX}$ (nm) (±5%)	16.4	15.2	25.0		174.4	
stirring	VT	MS	VT	MS	VT	MS
time (h)	36	36	36	36	72	36
major product of synthesis	ribbons	ribbons	tubes	ribbons	ribbons	tubes
major product after acid treatment	ribbons	ribbons	tubes	ribbons	tubes	tubes

[a] The type of stirring used is specified: vibrating table (VT) or magnetic stirring (MS). A thermal treatment (tt) on the soft chemistry (SC) specimen was necessary to obtain the anatase phase.

remain regarding the morphology, the structure, and the chemical composition of TNT.

The formation mechanism of TNT is also unclear. The assumption of the "peeling and rolling up" mechanism is often accepted.[17,24,25] In this process, the sodium titanate nanosheets probably start to grow inside the disordered phase (Ti, O, Na), obtained by TiO_6 octahedron dissolution. However, other hypotheses are suggested. Kukovecz et al. argue that TNT is formed by oriented crystal growth from nanoloop seeds.[26] Zhang et al. carried out calculations based on the density functional theory to explain the assumption of the "peeling and rolling" process:[27,28] hydrogen deficiency on one side of the surface layer of a $H_2Ti_3O_7$ plate would produce a driving force that enables the formation of nanotubes. Up to now, no study completely explained the formation mechanism of both tubes and by products (sheets, nanoribbons, etc.).

In this work, investigations are carried out with sharp correlation between several characterization techniques such as Raman spectroscopy, XRD, and high-resolution TEM (HR-TEM). The influence of the synthesis time, the grain size of the precursor, the type of stirring, and the acid treatment impact is discussed. The heterogeneity of the samples as well as both the morphology and the composition of the tubes are better understood by use of various analytical techniques.

2. Experimental Methods

2.1. Titanate Nanotubes and Nanoribbons Synthesis. TNT and nanoribbons were prepared by a classical hydrothermal method.[1,3] Various precursors were used. Anatase (laboratory manufacturing) prepared by soft chemistry followed by a thermal treatment at 300 and 500 °C (respectively, SC1 and SC2) (see ref 29 for more details), rutile (Tioxide), or P25 (Degussa) powders (440 mg) (Table 1) were added to a NaOH aqueous solution (10 mol/L, 110 mL). The mixture was transferred into a sealed Teflon reactor, and it was stirred either slowly by a vibrating table or more energetically by magnetic stirring during the synthesis. The hydrothermal reactor temperature was kept at 150 °C for 8, 36, or 72 h. Before and after the hydrothermal reaction, the pH was 13.4. The resulting white product was isolated by centrifugation and washed with distilled water until reaching neutral pH. Finally, the powder was freeze-dried. Acid treatments were realized on some samples in a 0.1 mol/L HCl solution for 30 min under magnetic stirring followed by distilled water washings and freeze-drying.

2.2. Characterization. TEM observations were performed on a JEOL JEM-2100 LaB_6 microscope operating at 200 kV and equipped with a high tilt pole piece achieving a point-to-point resolution of 0.25 nm. Raman spectra were recorded on a Jobin-Yvon T64000 microspectrometer with the 514.5 nm excitation line of an Ar−Kr laser. The laser beam was focused onto a 10 μm^2 area, and the power was kept below 1 mW to avoid sample heating.

An X-ray powder diffractometer INEL CPS 120 delivering the Cu Kα radiation ($\lambda = 1.5406$ Å) was used for measurements of powder diffraction patterns with high resolution. The crystallite size of the TiO_2 precursors was obtained using a Siemens D5000 diffractometer ($\theta/2\theta$, Cu Kβ radiation $\lambda = 1.39222$ Å) and using Bruker's Topas software. Peak position and desummation were obtained with the profile fitting program Profile available in the PC software package Diffrac AT supplied by Siemens. The desummation of each asymmetric peak was achieved by means of several symmetrical pseudo-Voigt functions.

XPS analyses were performed by a SIA 100 Riber/Cameca apparatus and a nonmonochromated Al Kα X-ray source (energy of 1486.6 eV, accelerating voltage of 12 kV, and power of 200 W). A Riber Mac 2 semi-imaging spectrometer was used with a resolution (measured from the Ag $3d_{5/2}$ line width) of 2.0 eV for global spectra and 1.3 eV for windows corresponding to selected lines. The spectrometer was used with its axis perpendicular to the surface of the sample. Preliminary analyses carried out with the aluminum source revealed interferences between the Auger titanium LMM peaks and the sodium 1s level. To bypass this problem, the magnesium source was used to quantify sodium. Samples were prepared by deposition of the powders on an indium sheet with $10 \times 10 \times 5$ mm^3 dimensions. Photoemission peak areas were calculated after background subtraction using a Shirley routine. Full widths at half-maximum were fixed for the fitting procedure: 1.7 eV for Ti $2p_{3/2}$ and 2.4 eV for Ti $2p_{1/2}$,[30] 1.6 eV for O^{2-}, 1.8 eV for OH^-, and 2.5 eV for H_2O component of O 1s peak. The carbon 1s peak (284.5 eV) allows correction of charge effects. According to measurements performed on standards, the concentration error is lower than 5%. The error is lower than 2% when repeating the measurements. From this point of view, the comparison between samples is very precise.

3. Results and Discussion

3.1. Heterogeneity of the Sample. We obtained heterogeneous products irrespective of the reaction time. This heterogeneity is seldom pointed out in the literature except in Thorne et al.[14] Our results showed that the formation of nanotubes was always accompanied by the formation of some byproducts such as amorphous phases, nanoribbons, or nanosheets (Figures 1 and 2). Figure 1 presents the different nanostructures obtained. The nanomaterials were classified into nanosheets and nanoribbons on the basis of their widths. Since it is difficult to determine a strict limit, from HRTEM, we defined these nanostructures with the help of interlayer distance perpendicular to the nanostructure axis. In nanosheets, this distance is always

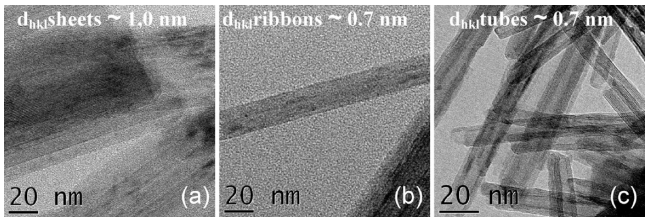

Figure 1. TEM images and typical d_{hkl} distance (perpendicularly to the nanostructure axis) of nanosheets, nanoribbons, and nanotubes synthesized (150 °C for 36 h) with (a, b) SC2 and (c) rutile precursor.

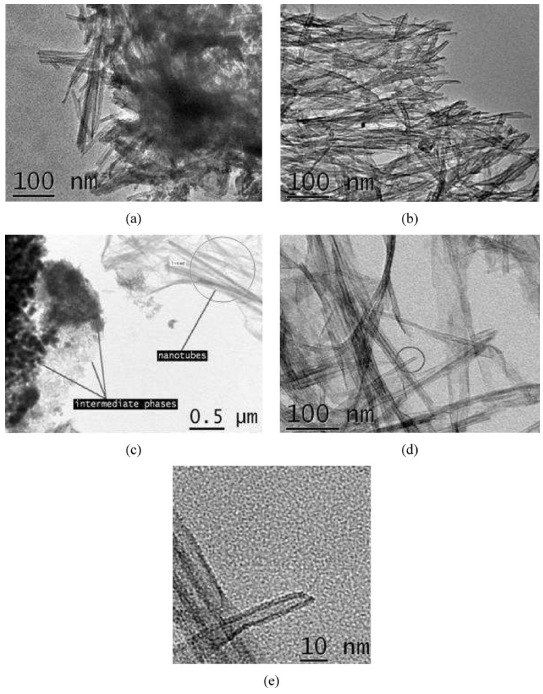

Figure 2. TEM images of nanotubes and intermediate phases obtained by hydrothermal treatment of P25 precursor after (a) 8 h at 150 °C, (b) 36 h at 150 °C, and (c−e) 72 h at 150 °C.

equal to 1.0 nm, whereas in nanoribbons and nanotubes it is 0.7 nm. This is an original and accurate way to clearly distinguish each kind of nanostructure (see section 3.4 for more details).

Regarding the yield study, only P25 precursor was used. The nanotube yield (qualitatively estimated by TEM) increased with increasing hydrothermal treatment time. However, the nanosheets are always present irrespective of the reaction time (Figure 2d). Consequently, even under the best hydrothermal synthesis conditions (72 h, 150 °C), a yield of 100% of nanotubes was never reached. This result is in agreement with that of Thorne et al. (after 72 h of hydrothermal treatment, only 80% of tube population was achieved).[14] It should be noted that increasing the synthesis time to 120 h did not increased the yield.

Raman microspectroscopy enabled us to reveal this heterogeneity in all the samples. Several spectra collected for each powder, in a 10 μm^3 volume, indicate two particular signatures: the first one is a weak signal (principal positions: 150.3, 188.2, 278.9, 447.4 cm^{-1}), and the second one displays narrow bands (principal positions: 158.5, 192.3, 263.3, 428.8 cm^{-1}) (Figure 3). These two kinds of spectra have already been published separately. A weak signal was measured on nanotubes obtained by Kukovecz et al.[18] The one with narrow bands seems similar to what was obtained on nanoribbons synthesized by Kolen'ko et al.[31] In this investigation, by repeating the Raman analysis

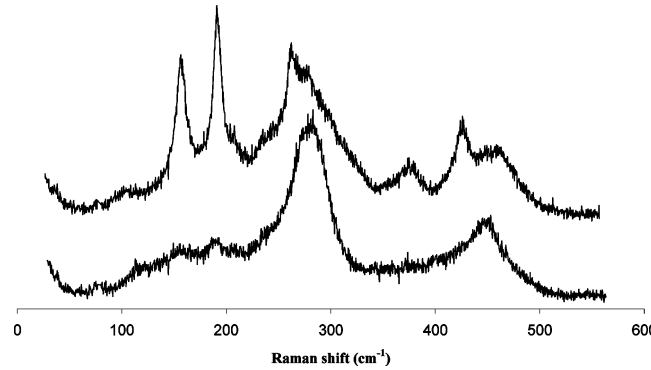

Figure 3. Raman spectra of titanate nanoribbons obtained after hydrothermal treatment (150 °C for 36 h) of TiO_2 anatase (SC1). These two spectra were recorded for 1000 s on the same sample.

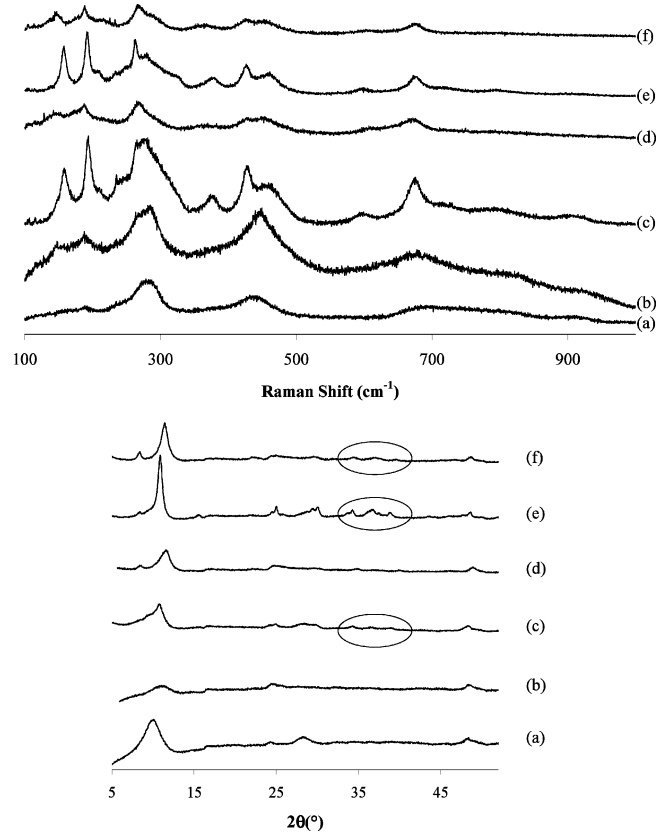

Figure 4. Raman spectra and XRD patterns of nanomaterials (nanosheets, nanoribbons, nanotubes) obtained starting from various precursors: (a, b) P25, (c, d) anatase SC1 homemade by soft chemistry, and (e, f) commercial rutile Tioxide and synthesized by a hydrothermal treatment at 150 °C for 36 h (P25, SC1) or 72 h (rutile Tioxide). (b, d, f) Obtained after acid treatment. Intensities are expressed in arbitrary units. Three small peaks appeared in the 33−40° 2θ position on XRD diffractograms when fine bands were observed on Raman spectra.

several times on a given sample, we observed the weak signal as well as the sharp peaks in both cases (i.e., when nanotubes were the main product (Figure 4a,f) and when nanoribbons were in majority (Figures 3 and 4c,e)). Raman results presented in Figure 4 are a statistically better representative pattern for each sample (for five measurements). Therefore, we could not conclude without ambiguity that weak signal is the signature of nanotubes and that fine signal is the signature of nanoribbons.

A correlation between Raman spectroscopy spectra and XRD diffractograms allows us to conclude that narrow bands are obtained on Raman spectra when three small peaks appear in

TABLE 2: XPS Chemical Element Ratio before and after Acid Treatment (0.1 mol/L HCl)[a]

				chemical element ratio			
precursor	synthesis time (h)	acid treatment	main product	Na/Ti	O^{2-}/Ti	OH^-/Ti	H_2O/Ti
P25	36	no	nanotubes	0.3	2.8	0.6	0.2
		yes	nanotubes	0.0	2.4	0.8	0.0
SC2	36	no	nanoribbons	2.5	2.6	0.5	0.2
		yes	nanoribbons	0.0	2.4	0.3	0.0
rutile	72	no	nanoribbons	2.1	1.6	1.3	0.2
		yes	nanotubes	0.1	2.4	0.6	0.0

[a] The use of new NaOH pellets between the first two and the last four syntheses may explain the difference found in sodium proportioning.

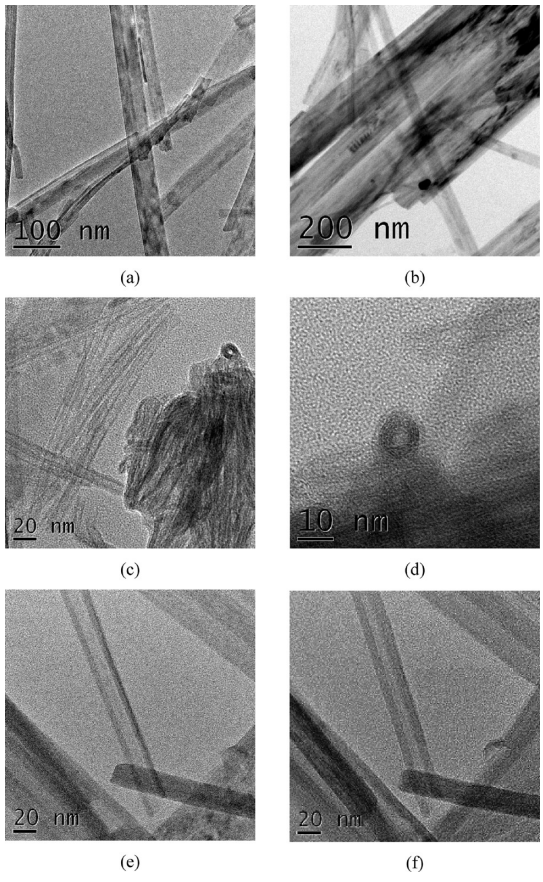

Figure 5. TEM images of (a, b) nanoribbons resulting from 72 h of commercial rutile hydrothermal treatment. (c−f) Nanotubes obtained from these nanoribbons thanks to an acid treatment (HCl 0.1 mol/L). (d) Nanotube cross section. (f) Tilted image of (e) (40°).

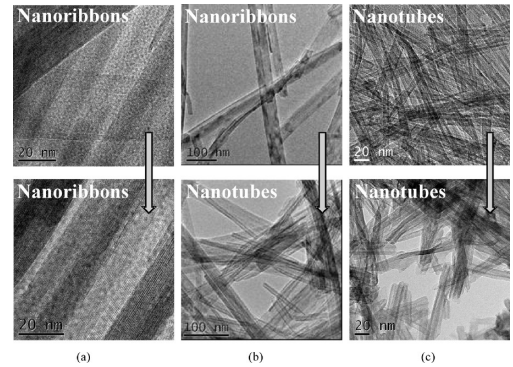

Figure 6. Morphological evolution before and after acid treatment: (a) titanate nanoribbons stay nanoribbons (P25 precursor under magnetic stirring), (b) titanate nanoribbons change into nanotubes (rutile precursor under vibrating stirring), and (c) titanate nanotubes stay nanotubes (rutile precursor under magnetic stirring).

the 33−40° 2θ position on XRD diffractograms (λK_β Cu = 1.39222 Å, Figure 4c,e,f). These three small peaks have not been clearly attributed up to now. They could be assigned respectively to the (301) and (501) reflections of $H_2Ti_2O_5 \cdot H_2O$ (47-0124 ICDD card) and the ($60\bar{2}$) reflection of $H_2Ti_3O_7$ (47-0561 ICDD databank).

Moreover, there is no clear correlation between the chemical composition of these nanostructures, determined by XPS spectroscopy (Table 2), and their Raman signature. Indeed, we are going to show in the next section that this composition changes after acid treatment, whereas the narrow bands of Raman spectra appeared irrespective of these conditions (i.e., before and after the washings).

All these correlated results show that the formation of nanotubes was accompanied by the formation of some byproducts such as amorphous phases, nanoribbons, or nanosheets. These byproducts are different in their morphologies and chemical compositions. Synthesizing 100% nanotubes without having any byproduct is still a challenge. These results also showed that it is difficult to correlate the Raman and XPS spectra to each nanostructure, and some results are still not clearly understood.

3.2. Impact of Acid Treatment and Stirring. TNT was obtained directly, without acid treatment, starting from P25 (Figure 2) or rutile precursor (Table 1) when a vibrating table and a nonvigorous magnetic stirring, respectively, were applied. However, the acid treatment turned out to be necessary when the first step of the hydrothermal treatment was not sufficient to obtain nanotubes. For the rutile raw material and using a vibrating table instead of magnetic stirring, nanoribbons were first synthesized and then by the acid treatment (0.1 mol/L HCl) they were converted into nanotubes in a second step (Figures 5 and 6). However, ribbons do not always change into tubes when SC1, SC2, and P25 precursors were used (Table 1).

The stirring impact seems to be a very important parameter that is never discussed in the literature. It appears that nonvigorous stirring is required to obtain a higher yield of real crystallized tubes. Without stirring or with vigorous magnetic stirring, the amount of transformation into tubes is low. Two types of slow stirring were then considered: vibrating table and moderate magnetic stirring. The selection of the mode of stirring was dependent on the precursor used; for example, P25 precursor nanotubes were obtained when vibrating table was used, whereas nanoribbons resulted in the case of magnetic stirring (Table 1).

Concerning the impact of acid washing, XPS analyses revealed several major changes. First, we should note that analyses were carried out under ultrahigh vacuum. As a consequence, the water identified from the O 1s peak referred to structural water and not to physically or chemically adsorbed water. In addition to this structural water component, oxygen peak contributions are crystal lattice and hydroxide oxygens. During acid washing, the O 1s peak lost its H_2O component

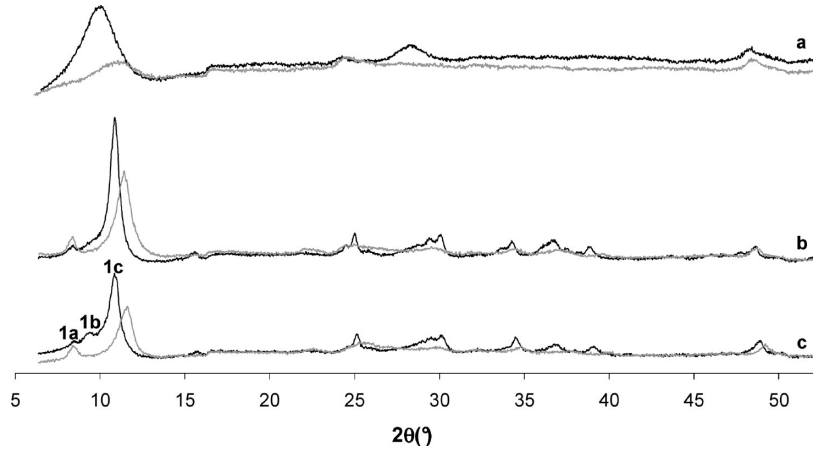

Figure 7. Powder X-ray diffraction patterns before (black) and after (gray) acid treatment: (a) titanate nanotubes remain nanotubes (P25 precursor), (b) titanate nanoribbons change into nanotubes (rutile precursor), and (c) titanate nanoribbons stay nanoribbons (soft chemistry precursor SC2). The first peak incorporates several components (1a, 1b, 1c).

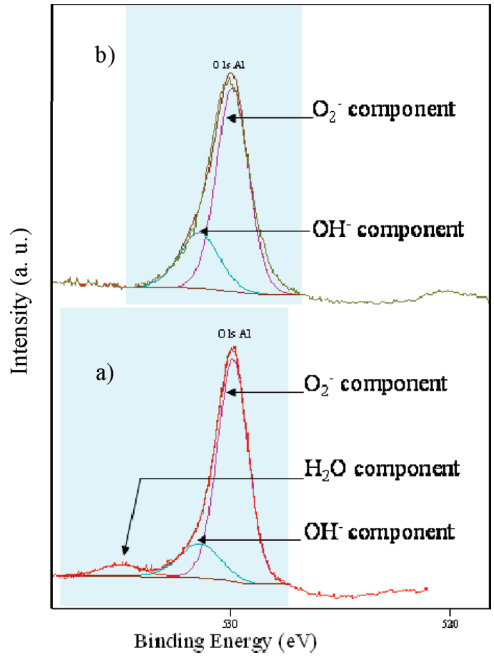

Figure 8. O 1s XPS peak of titanate nanotubes obtained with P25 starting material: (a) after a hydrothermal synthesis for 36 h, and (b) after a hydrothermal synthesis for 36 h and an acid treatment.

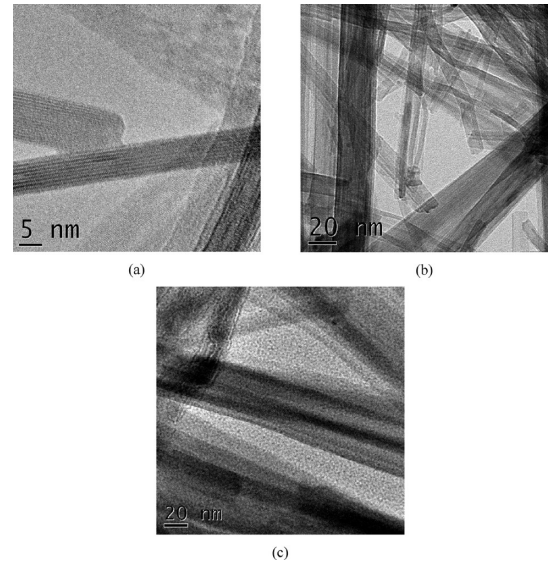

Figure 9. TEM images of nanoribbons obtained by a 150 °C hydrothermal treatment of TiO_2: (a) precursor SC1 for 36 h, (b) precursor SC1 for 72 h, and (c) precursor SC2 for 36 h.

(located at 535.0 eV) (Figure 8), and the Na 1s peak also disappeared. This result may be explained by the substitution of Na^+ ions by H^+ ions during the acid treatment. Resulting steric hindrance present between nanotube walls becomes lower than in the case of the structural water and Na^+ presence. This remark is accredited by the XRD results concerning the decrease of the distance between nanotube walls. Indeed, whatever the morphological change produced by the acid treatment, a shift of the first XRD peaks (1a, 1b, 1c) was always observed (Figure 7). This shift was toward higher 2θ, which means smaller interplanar distances. Since the first peak was related to the distance between tube walls along the tube axis, this interlayer distance decreased after acid washing. In addition, the peak around $2\theta = 28-30°$ disappeared with HCl treatment. This peak is consistent with the (310) reflection of $H_2Ti_2O_5 \cdot H_2O$ (47-0124 ICDD card). Since it is a reflection coming from a hydrate, if these plans are related to H_2O positions in the lattice, they may be more affected by acid washing (water elimination).

Using the Na 1s, O 1s, and Ti $2p_{3/2}$ levels, we determined the atomic ratios of several samples (Table 2). The O^{2-}/Ti ratio was not in good agreement with the supposed $Na_2Ti_3O_7$ or $H_2Ti_3O_7$ composition of the nanostructure before the acid washing but it became close to the expected 2.33 ratio after. The amount of sodium, before the acid washing, was very different for each synthesis and very different with the expected 0.67 Na/Ti ratio of the supposed $Na_2Ti_3O_7$ composition. This variation is not related to synthesis time, nor to the chosen precursors or to final morphology, but it may be related to the purity of the base. Indeed, large amounts of sodium were obtained with a fresh base; in contrast, low amount were obtained with an old one (more carbonated). Nevertheless, we can notice that the tubes always contain a small amount of sodium (Table 2, in agreement with Chen et al.[16]). Intermediaries such as sheets and ribbons contain more sodium. This is to be correlated with the influence of acid washings which eliminate sodium and tend to form tubes. Finally, the H_2O/Ti ratio is always closed to 0.2 before the acid washing and the evolution of the OH^-/Ti ratio could not be simply explained.

The heterogeneous nature of our samples makes it difficult to interpret the micro-Raman spectra. A shift of the two first peak positions is observed after the acid treatment (i.e., 158.54 and 192.26 cm^{-1} positions toward 147.18 and 189.54 cm^{-1}

TABLE 3: XRD and TEM d_{hkl} Results for Nanostructures Prepared from Various Precursors (See Table 1)[a]

precursors	synthesis time and major product (T = tubes, R = ribbons)	*d* 1a (nm)			*d* 1b (nm)			*d* 1c (nm)			*d* 2 (nm)			area ratio $S_{1a}/(S_{1a}+S_{1b}+S_{1c})$(%)
		HRTEM	XRD	area (au)	HRTEM	XRD	area (au)	HRTEM	XRD	area (au)	HRTEM	XRD	area (au)	
P25 (Degussa)	36 h → T		1.00	1721		0.88	13482	0.75	0.78	1432		0.37	502	10.3
	72 h → T		1.06	471		0.92	343	0.71	0.80	7500	0.37	0.36	4318	5.7
SC1 (tt 15 h, 300 °C)	36 h → R		1.07	962		0.91	3612	0.73	0.81	6357	0.36	0.36	1197	8.8
	72 h → R	1.00	1.08	4446		0.87	12579	0.75				0.37	2358	32.9
SC2 (tt 2 h, 500 °C)	36 h → R	1.00	1.05	1389		0.86 and 0.94	804 and 4415	0.69 and 0.74	0.80 and 0.81	482 and 6671		0.30 and 0.35	10129 and 1672	10.1
	36 h + acid → R	1.05	1.05	1201				0.69 and 0.73	0.76 and 0.79	3156 and 5237		0.30, 0.35 and 0.39	3677, 3087, and 295	12.5
rutile (Tioxide)	72 h → R	1.00 and 1.02	1.06	1599		0.87	3395	0.72	0.81	10783		0.35 and 0.36	983 and 533	10.1
	72 h + acid → T	1.07	1.06	1261				0.70 and 0.82	0.77 and 0.79	8506 and 3129		0.30, 0.33, 0.36, 0.39, and 0.40	1719, 1294, 1662, 220, and 657	9.8

[a] tt = thermal treatment. The *d* 1b distance revealed by XRD, of about 0.90 nm, could not be distinguished from those of 1.00 by HRTEM because of the resolution of the apparatus used (0.25 nm). Several values appeared in XRD results when it was not possible to decompose the peak in only one component. For example, for *d* 1b and *d* 1c, the desummation was sometimes better with two peaks instead of one. *d* 2, corresponding to the peak at about 22°, was sometimes the superposition of at least five components.

positions in the case of Figure 4e,f). The origin of this shift was still not clearly identified.

3.3. Precursor Size Effect. Since the influence of precursor size on morphology of the nanomaterial was not clearly understood, we evaluated four different TiO_2 precursors in this study. Their grain size, determined by several techniques, varied from 15 to 175 nm (Table 1).

Nanotubes were only obtained, whatever the synthesis conditions (reaction time, stirring mode, acid washing), when the starting precursors had grain sizes larger than 25 nm and when the rutile structure which is the thermodynamically stable structure for such large grain sizes is present.[32] Nanotubes were never obtained when nanometric particles of anatase, with sizes smaller than 17 nm, were used (SC1 and SC2, Table 1). This is an interesting discovery because up to now it was assumed that it was always possible to obtain nanotubes with crystalline precursors.[16] Our precursors were not amorphous; they were just too small to lead to the construction of nanotubes during the hydrothermal treatment. When anatase nanoparticles of 15−16 nm were used as precursor, nanoribbons were obtained in majority, whatever the synthesis time (36 h, 72 h, etc.) (Figure 9).

It is well-known that dissolution/recrystallization phenomena depend on the size of primary germs. Therefore, for a very small TiO_2 precursor, there could be too many germs leading to the nonobtainment of supersaturation necessary for the growth of the nanotubes. The number of nucleation sites may also be more important. All these remarks may explain why it is difficult to obtain an important crystal growth necessary for the obtainment of nanotubes (before the ruling step). This may explain why nanoribbons (with smaller width) are mainly obtained.

The size of the precursor is a determining parameter to obtain nanotubes or nanoribbons.

3.4. Desummation of the XRD Peaks: A Way To Quantify the Byproduct. As previously mentioned, the structure and the chemical composition of titanate products (nanotubes or nanoribbons) are still not clearly defined. For example, even if the diffractograms of the powders obtained in this study are similar to those mentioned in literature, none of them perfectly matched those of the International Center for Diffraction Data (ICDD) databank cards. Our patterns are the superposition of at least three components: $H_2Ti_5O_{11}\cdot 3H_2O$ (44-0130 ICDD card, monoclinic system, space group *C*2/*m*), $H_2Ti_3O_7$ (47-0561 ICDD card, monoclinic system, space group *C*2/*m*), and $H_2Ti_2O_5\cdot H_2O$ (47-0124 ICDD card, orthorhombic system). For this reason, we do not index the whole diffractogram.

According to the literature, the first peak is characteristic of the distance between two consecutive tube walls. The other peaks are less easy to understand. Indeed, harmonic position calculations (i.e., possible multiple 2θ positions for a same "*d*") could not explain the remaining peaks of our diffractograms. In the hypothesis of pure and perfect nanotubes ($H_2Ti_3O_7$ nanotubes model), Chen et al.[16] simulated an XRD pattern. In their case, the simulated and experimental diffractograms perfectly matched. Considering the heterogeneities always present in all samples, no simulation was realized. To get a better understanding of these complex nanostructures, mixture of nanotubes, nanoribbons, and nanosheets, a careful estimation of the crystallographic distances was made by both TEM and XRD. Inter-reticular distances were deduced from Fourier transform of high-resolution micrographies. Obviously, the value of these distances is independent of the azimuth of the sample, which is not the case for distances corresponding to the internal and external diameter of the nanotubes. In Table 3, a non-

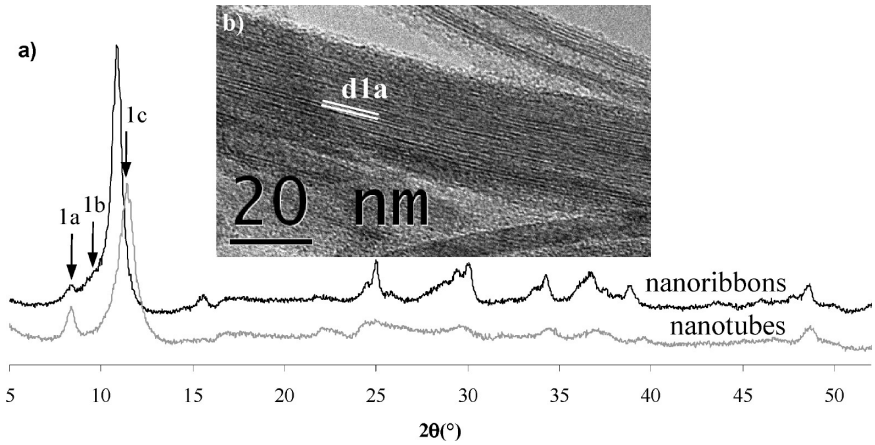

Figure 10. (a) XRD patterns of titanate nanoribbons and nanotubes synthesized 72 h with rutile precursor (with or without acid washing). The first peak incorporates three components (1a, 1b, 1c). (b) HRTEM image of sheets present in the sample (byproduct of the reaction).

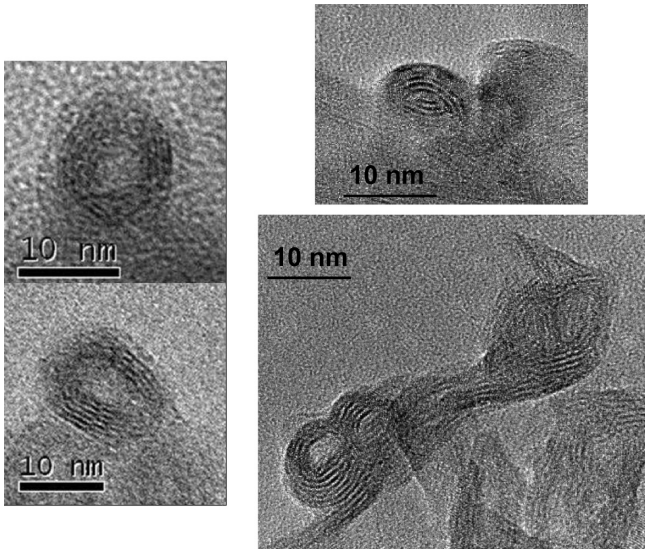

Figure 11. HRTEM sections of titanate nanotubes (obtained with rutile precursor).

exhaustive list of interplanar distances, extracted from HRTEM micrographs, was collected to compare them with d_{hkl} coming from XRD patterns. It appears that the distances around 0.7 and 0.36 nm were only observed on nanotubes or nanoribbons (not on nanosheets). As said previously, in nanosheets, the interplanar distance was always close to 1.0 nm. This interlayer spacing is consistent with the interlayer spacing d_{200} in $H_2Ti_5O_{11}\cdot 3H_2O$ (1.04 nm, 44-0130 ICDD databank). This distance is not present in other classical structures ($H_2Ti_3O_7$, $Na_2Ti_3O_7$, $H_2Ti_2O_5\cdot H_2O$).

A precise desummation of the first peak revealed that for most samples this peak (Figures 7 and 10) incorporated several components, up to three (1a, 1b, 1c, Table 3) with the following average positions: 1.04, 0.90, and 0.79 nm (depending on the samples). For instance, in Figures 7 and 10, this peak clearly showed some asymmetry at low angles. Since this asymmetry was not present for every sample and remained whatever the XRD apparatus used (curve sensitive detector, $\theta/2\theta$ detector, etc.), it cannot be attributed to an instrumental aberration and is due to the heterogeneity of the samples. This observation, never mentioned in the literature, can nevertheless be observed in XRD patterns of other authors. For instance, in Figure 2 of ref 33 the first peak clearly shows some asymmetries. To perform XRD refinements, a simple model taking into account several phases (in general three) was used. The decomposition of each asymmetric peak can be achieved by means of several symmetrical pseudo-Voigt functions.

As previously said, the HRTEM average distance of 1.04 nm, corresponding to the *d* 1a distance in XRD patterns (Figure 10a), was only located in the case of sheet byproducts, which were present in a lot of specimens, even after three days of hydrothermal treatment. The *d* 1b and *d* 1c distances of about 0.9 and 0.8 nm, respectively, correspond to both distances between two consecutive walls in nanotubes and to an interplanar distance in nanoribbons. This value is almost the same as the interlayer spacing d_{200} in $H_2Ti_3O_7$ (0.79 nm, 47-0561 ICDD databank); this value is to be compared with the one for $Na_2Ti_3O_7$ (d_{001} = 0.84 nm, 01-070-9440 ICDD databank, monoclinic system, SG $P2_1/m$). Even if these d_{hkl} distances are very close for both nanotubes and nanoribbons, we clearly separate these two morphologies by HRTEM, because of the presence of the inner cavity for tubes. Concerning the names "nanoribbons" and "nanosheets", we always measure distances of 1.0 and 0.7 nm, respectively, on nanosheets and nanoribbons. Moreover, we can notice that the width of nanosheets is always much higher than 20 nm. As a consequence, we are able to distinguish these three morphologies.

We already pointed out that a nanotube ratio of 100% remains difficult to reach. The presence of byproduct (i.e., nanoribbons, nanosheets, and original precursor) can be a drawback for future applications. Thus, the estimate of the proportion of each nanostructure is of importance. Up to now, the nanotube proportion has only been estimated by TEM. This method is rather qualitative, and an accurate quantification would require a long time of investigation. Moreover, with this technique, it is hard to be sure that what is observed is representative of the entire products. For these reasons, we tried to develop a more accurate method based on previous observations and remarks (Table 3 and Figures 7 and 10). The analysis of XRD patterns is a quantitative way to estimate the amount of sheets (contribution at 1 nm in the desummated first peak).

By this methodology, it appears that, in the case of the rutile precursor under vibrating stirring and before acid treatment, the peak surface ratio (1a)/(1a + 1b + 1c) gives a 10% quantity of sheets. After acid treatment, one can notice a shift of the first peaks but also a constant peak surface ratio (1a)/(1a + 1b + 1c) showing that the amount of sheets is still 10%. The major product was nanoribbons before acid treatment and nanotubes after the treatment. As the amount of nanosheets is the same

before and after acid treatment, the change of the nature of the major product only comes from nanoribbons that turned into nanotubes.

The influence of synthesis time on the sheets ratio is complex. In the case of P25 precursor, it seems that it decreases from 10 to 6% when residence time increases (36 to 72 h). Contrary to SC1 precursor, the proportion of sheets increases from 9% after 36 h to 33% after 72 h.

For the first time, a careful desummation of the first XRD peak revealed the presence of both nanosheets and nanotubes/nanoribbons and allowed an estimation of their proportions.

3.5. Flattened Morphology of the Nanotubes. We have already seen that TNT has a multilayer morphology, rolled up in spiral. The length can reach a few hundred nanometers and their diameter only a few nanometers, in our case up to approximately 20 nm under hydrothermal syntheses conditions ($3-4$ nm $< d_{inner} <$ 10 and 10 nm $< d_{outside} <$ 20 nm). For the first time, an original observation has been done: The tubes are not perfectly cylindrical in shape (Figure 11). They sometimes have an ellipsoidal section. This result was confirmed by tilting the nanotube (Figure 5e,f). By tilting, the thickness of the wall gets modified. On the first TEM image (Figure 5e), an outside diameter of 20.2 nm and an inner diameter of 9.7 nm were observed. On the second one (Figure 5f), after tilting by 40°, these diameters were, respectively, 22.5 and 6.0 nm. These distances were deduced from a profile of intensity of gray levels of the section of the nanotubes (both in flat and tilted cases). Since grinding was not used, the preparation of the sample could not be held responsible for this flattened morphology. As a result, this particular morphology may help distinguish between various formation mechanisms.

4. Conclusions

Titanate nanotubes, nanoribbons, and nanosheets remain a matter of discussion since the pioneering works of Kasuga et al. In particular, several differences are regularly noticed even when the nanostructures are synthesized under very similar conditions in the nanomaterial morphologies, nanotube crystallographic structure, and their chemical compositions. These controversies are partly due to the heterogeneities present in all the samples and rarely considered in the literature. Indeed, thanks to TEM, XRD, and micro-Raman spectroscopy, several morphologies and structures were characterized in all the samples.

Moreover, it was illustrated that the first acid treatment resulted in an elimination of any trace of sodium and structural water. The second effect of acid washing is a morphological evolution: nanoribbons become nanotubes. Moreover, nanotubes obtained after the hydrothermal treatment showed a slight change in their interlayer distance after the acid treatment as illustrated by XRD.

For the first time, a careful desummation of the first XRD peaks revealed the presence of both nanosheets and nanotubes/nanoribbons and allowed an estimation of their proportions. In addition, a flattened structure was revealed by HRTEM observations. Some titanium oxide nanotubes sections are not perfectly circular but rather elliptical.

References and Notes

(1) Kasuga, T.; Hiramatsu, M.; Hoson, A.; Sekino, T.; Niihara, K. *Langmuir* **1998**, *14*, 3160–3163.
(2) Kasuga, T.; Hiramatsu, M.; Hoson, A.; Sekino, T.; Niihara, K. *Adv. Mater.* **1999**, *11*, 1307–1311.
(3) Bavykin, D. V.; Lapkin, A. A.; Plucinski, P. K.; Friedrich, J. M.; Walsh, F. C. *J. Phys. Chem. B* **2005**, *109*, 19422–19427.
(4) Armstrong, G.; Armstrong, A. R.; Canales, J.; Brucea, P. G. *Electrochem. Solid-State Lett.* **2006**, *9*, A139−A143.
(5) Li, J.; Tang, Z.; Zhang, Z. *Electrochem. Commun.* **2005**, *7*, 62–67.
(6) Fu, L. J.; Liu, H.; Li, C.; Wu, Y. P.; Rahm, E.; Holze, R.; Wu, H. Q. *Prog. Mater. Sci.* **2005**, *50*, 881–928.
(7) Xu, H.; Konishi, H.; Yeredla, R. R.; Wang, Y. Abstracts of Papers, 233rd National Meeting of the American Chemical Society, Chicago, IL, March 25−29, 2007; American Chemical Society: Washington, DC, 2007.
(8) Adachi, M.; Murata, Y.; Okada, I.; Yoshikawa, S. *J. Electrochem. Soc.* **2003**, *150*, 488–493.
(9) Kim, W. Y.; Kang, Y.; Kim, D. *Diffus. Defect Data, Pt. B* **2007**, 124–126.
(10) Mor, G. K.; Varghese, O. K.; Paulose, M.; Grimes, C. A. *Sens. Lett.* **2003**, *1*, 42–46.
(11) Oh, S. H.; Finones, R. R.; Daraio, C.; Chen, L. H.; Jin, S. *Biomaterials* **2005**, *26*, 4938–4943.
(12) Liu, A.; Wei, M.; Honma, I.; Zhou, H. *Adv. Funct. Mater.* **2006**, *16*, 371–376.
(13) Yuan, Z.-Y.; Su, B.-L. *Colloids Surf., A* **2004**, *241*, 173–183.
(14) Thorne, A.; Kruth, A.; Tunstall, D.; Irvine, J. T. S.; Zhou, W. *J. Phys. Chem. B* **2005**, *109*, 5439–5444.
(15) Du, G. H.; Chen, Q.; Che, R. C.; Yuan, Z. Y.; Peng, L. M. *Appl. Phys. Lett.* **2001**, *79*, 3702–3704.
(16) Chen, Q.; Zhou, W.; Du, G.; Peng, L. M. *Adv. Mater.* **2002**, *14*, 1208–1211.
(17) Li, W.; Fu, T.; Xie, F.; Yu, S.; He, S. *Mater. Lett.* **2007**, *61*, 730–735.
(18) Kukovecz, A.; Hodos, M.; Konya, Z.; Kiricsi, I. *Chem. Phys. Lett.* **2005**, *411*, 445–449.
(19) Ma, Y.; Lin, Y.; Xiao, X.; Zhou, X.; Li, X. *Mater. Res. Bull.* **2006**, *41*, 237–243.
(20) Nakahira, A.; Kato, W.; Tamai, M.; Isshiki, T.; Nishio, K.; Aritani, H. *J. Mater. Sci.* **2004**, *39*, 4239–4245.
(21) Ma, R.; Bando, Y.; Sasaki, T. *Chem. Phys. Lett.* **2003**, *380*, 577–582.
(22) Sun, X.; Li, Y. *Chem.−Eur. J.* **2003**, *9*, 2229–2238.
(23) Yoshida, R.; Suzuki, Y.; Yoshikawa, S. *Mater. Chem. Phys.* **2005**, *91*, 409–416.
(24) Chen, Y. F.; Lee, C. H.; Yeng, M. Y.; Chiu, H. T. *Mater. Chem. Phys.* **2003**, *81*, 39–44.
(25) Wang, Y. Q.; Hu, G. Q.; Duan, X. F.; Sun, H. L.; Xue, Q. K. *Chem. Phys. Lett.* **2002**, *365*, 427–431.
(26) Kukovecz, A.; Hodos, M.; Horvath, E.; Radnoczi, G.; Konya, Z.; Kiricsi, I. *J. Phys. Chem. B* **2005**, *109*, 17781–17783.
(27) Zhang, S.; Peng, L.-M.; Chen, Q.; Du, G. H.; Dawson, G.; Zhou, W. Z. *Phys. Rev. Lett.* **2003**, *91*, 256103.
(28) Zhang, S.; Chen, Q.; Peng, L. M. *Phys. Rev. B* **2005**, *71*, 014104.
(29) Pighini, C.; Aymes, D.; Millot, N.; Saviot, L. *J. Nanopart. Res.* **2007**, *9*, 309–315.
(30) Pétigny, S.; Mostéfa-Sba, H.; Domenichini, B.; Lesniewska, E.; Steinbrunn, A.; Bourgeois, S. *Surf. Sci.* **1998**, *410*, 250–257.
(31) Kolen'ko, Y. V.; Kovnir, K. A.; Gavrilov, A. I.; Garshev, A. V.; Frantti, J.; Lebedev, O. I.; Churagulov, B. R.; Tendeloo, G. V.; Yoshimura, M. *J. Phys. Chem. B* **2006**, *110*, 4030–4038.
(32) Navrotsky, A. *Geochem. Trans.* **2003**, *4*, 34–37.
(33) Ma, R.; Fukuda, K.; Sasaki, T.; Osada, M.; Bando, Y. *J. Phys. Chem. B* **2005**, *109*, 6210–6214.

JP903195H